Journal of Geophysical Research: Earth Surface

RESEARCH ARTICLE
10.1029/2018JF004680

Glacial Erosion Driven by Variations in Meltwater Drainage

S. V. Ugelvig[1], D. L. Egholm[1], R. S. Anderson[2], and N. R. Iverson[3]

[1]Department of Geoscience, Aarhus University, Aarhus, Denmark, [2]Institute of Arctic and Alpine Research (INSTAAR) and Department of Geological Sciences, University of Colorado, Boulder, CO, USA, [3]Department of Geological and Atmospheric Sciences, Iowa State University, Ames, IA, USA

Key Points:
- We model the influence of glacial hydrology on rates of subglacial abrasion and quarrying
- The model experiments record the ice-bed contact area and stress over time and use these to predict rates of basal sliding and erosion
- Our experiments show that meltwater variability consistently accelerates glacial erosion

Supporting Information:
- Supporting Information S1
- Data Set S1

Correspondence to:
D. L. Egholm,
david@geo.au.dk

Citation:
Ugelvig, S. V., Egholm, D. L., Anderson, R. S., & Iverson, N. R. (2018). Glacial erosion driven by variations in meltwater drainage. *Journal of Geophysical Research: Earth Surface*, *123*, 2863–2877. https://doi.org/10.1029/2018JF004680

Received 16 MAR 2018
Accepted 10 OCT 2018
Accepted article online 31 OCT 2018
Published online 12 NOV 2018

Abstract The subglacial processes of abrasion and quarrying are thought to be primarily responsible for bedrock erosion by glaciers. While theory points to sliding speed as the dominant control on abrasion, rates of quarrying are likely scaled by a more complex combination of sliding speed, effective pressure, bed roughness, and short-term water-pressure fluctuations. Here we pair a model for quarrying based on statistical characterization of bedrock strength with a model for subglacial hydrology that describes the temporal evolution of cavities under the influence of variations in sliding speed and effective pressure. Using a finite element model, we simulate the evolution of the hydrological system at the base of a glacier and compute rates of abrasion and quarrying. Cavity lengths and channel cross sections evolve through time, causing temporal shifts in ice-bed contact area, which in turn govern the differential stress that influences erosion over the course of a year. Our results demonstrate how variations in meltwater production amplify rates of subglacial erosion relative to the case of steady meltwater generation. The level of amplification depends on how the variations control the ice-bed contact area. Seasonal variations are most effective in boosting mean rates of basal sliding and hence subglacial abrasion, whereas shorter-term variations (monthly-weekly) most strongly influence rates of subglacial quarrying through temporal amplification of differential bedrock stress around cavities. This influence of transient hydrology on subglacial erosion processes may explain why glaciers in temperate climates with strong variations in temperature and precipitation erode faster than similar-type glaciers in polar environments.

1. Introduction

Subglacial hydrology controls rates and patterns of subglacial erosion, in part due to the influence of water pressure on rates of basal sliding (Bartholomaus et al., 2008; 2011; Hallet, 1979; Herman et al., 2011; Iverson, 1991; Koppes et al., 2015). The two dominant subglacial erosion processes, abrasion and quarrying, are both partially controlled by sliding speed, and quarrying is further influenced by the effective ice-bed contact pressure as well as by short-term water pressure fluctuations (Anderson, 2014; Cohen et al., 2006; Hallet, 1979; Hallet, 1996; Iverson, 1991, 2012). Hence, when quantifying and modeling subglacial erosional processes, the hydrological model used must capture first-order behavior of the subglacial hydrological system (e.g., De Fleurian et al., 2014; Flowers & Clarke, 2002; Hewitt, 2013; Kessler & Anderson, 2004; Schoof, 2010; Werder et al., 2013).

Glacial landscape evolution models usually assume that rates of subglacial erosion simply scale with some power of the sliding speed, and this assumption can indeed lead to realistic glacial landforms when erosion is integrated over time (Anderson et al., 2006; Egholm et al., 2009, 2012, 2017; Herman et al., 2011; Hildes et al., 2004; Jamieson et al., 2008; Kessler et al., 2008; MacGregor et al., 2000; Tomkin, 2009). However, empirical studies show that bedrock strength, climate variability, and glacier size may be of equal importance in setting the pace of erosion (Cohen et al., 2006; Dühnforth et al., 2010; Hallet, 1996; Hooyer et al., 2012; Koppes et al., 2015). Although theoretical models for abrasion emphasize the primary role of sliding speed, both for determining the flux of debris moving over bedrock and for scaling the contact force between debris and bedrock (Hallet, 1979; Iverson, 1990), rates of quarrying are likely limited foremost by the conditions that control cavity formation along the glacier bed, among which basal sliding speed plays only a partial role (Anderson, 2014; Cohen et al., 2006; Hallet, 1996; Hildes et al., 2004; Iverson, 1991, 2012; Ugelvig et al., 2016).

Studies investigating the factors that control quarrying have employed different strategies and assumptions (Anderson, 2014; Cohen et al., 2006; Hallet, 1996; Hildes et al., 2004; Iverson, 1991, 2012; Ugelvig et al., 2016).

Figure 1. Photo from the forefield of Castleguard Glacier, an outlet of the Columbia Icefield in northern Banff National Park, Alberta, Canada. The rock is subhorizontally bedded limestone. Note the staircase-style topography. Photo by Keith Williams.

Early work of Iverson (1991) and Hallet (1996) focused on the temporal evolution of stress in homogeneous bedrock with only small isolated cracks. Assuming that quarrying rate scales with crack growth rate, they found the fastest quarrying to occur at times when water pressure drops faster than ice creep can reduce cavity size, thereby shifting some of the weight of the glacier from water in cavities to the adjacent rock where the differential stress consequently increases (Hallet, 1996; Iverson, 1991). Experiments by Cohen et al. (2006) at Svartisen Subglacial Laboratory later confirmed that rapid water-pressure fluctuations can drive crack growth in rock.

However, deglaciated bedrock (Figure 1) seldom contains only minor isolated cracks (Becker et al., 2014; Dühnforth et al., 2010; Hooyer et al., 2012; Krabbendam & Bradwell, 2014), and preexisting fractures and joints are known to control both the rate and spatial distribution of quarrying (Becker et al., 2014; Dühnforth et al., 2010; Hooyer et al., 2012). Hence, to account for preexisting fractures in a model of quarrying, Iverson (2012) introduced a statistical description of bedrock strength. Like earlier models (Hallet, 1996; Iverson, 1991) a staircase bed geometry was considered with step length, L_s, and step height, h. The probability, k, of a step being quarried was described using Weibull theory for the distribution of flaws:

$$k = 1 - \exp\left[-\frac{h(L_s - S)}{V_0}\left(\frac{\sigma_d}{\kappa\sigma_0}\right)^m\right] \tag{1}$$

Here S is cavity length; V_0 is a characteristic rock volume sufficiently large to contain the rock's largest fractures (Table 1); σ_0 is the Weibull scale parameter, which approximates the mean tensile strength of the rock; κ is a factor reducing σ_0 to account for the smaller stresses required for slow subglacial crack growth than for the rapid crack growth of laboratory tests; m is the Weibull modulus, which decreases with increasing strength heterogeneity of the rock, and σ_d is the differential bedrock stress (the difference between the stresses applied on different faces of a bedrock block). This model of bedrock strength is based on the assumption that larger rock masses have less strength because they are more likely to contain large fractures (Jaeger & Cook, 1979). This dependency on glacially stressed bedrock volume is reflected in the factor $(L_s - S)/V_0$ in equation (1) (hereafter called the "volume factor"). The other term $(\sigma_d/(\kappa\sigma_0))^m$ (hereafter referred to as the

Table 1
Model Parameters

Symbol	Description	Value
Ice model		
B	Viscosity constant	73.3×10^6 Pa $s^{1/3}$
n	Ice stress exponent	3.0
ρ_i	Density of ice	910 kg m^{-3}
L_i	Ice latent heat of fusion	3.34×10^5 J kg^{-1}
K_s	Creep-sliding parameter	18.3×10^6 Pa $s^{1/3}$
τ_s	Regional horizontal shear stress	134 kPa
Hydrology model		
ρ_w	Density of water	1000 kg m^{-3}
c_t	Transmissivity	1×10^{-3} $kg^{-1/2}$ $m^{3/2}$
α	Flux parameter	5/4
β	Cavity shape parameter	0.7
L_c	Channel width (grid resolution)	25 m
e_G	Englacial void ratio	10^{-3}
k_0	Boundary flux parameter	15×10^3 m
Erosion model		
K_a	Abrasion constant	10^{-7} y m^{-1}
κ	Rate scaling factor	1/3
c	Stress scaling factor	0.1
σ_0	Weibull scale parameter	10 MPa
σ_n^*	Brittle yield stress of ice	10 MPa
V_0	Characteristic volume per unit width	10 m^2
m	Weibull modulus	3
Topography model		
λ	Wavelength of variation	100 m
A_t	Amplitude of variation	20 m
ν	Hurst exponent	0.5
S_r	Regional slope	5%

"differential stress factor") describes how the level of bedrock differential stress influences the probability of quarrying for a given degree of bedrock strength heterogeneity. The differential stress, σ_d, typically increases when cavities grow and the load of the ice must be supported by a smaller area of the bed. Thus, the volume factor and the differential stress factor have opposing dependencies on ice-bed contact area.

Iverson's (2012) quarrying model has, so far, been used only in simulations with cavities of steady state size (Beaud et al., 2014; Iverson, 2012; Ugelvig et al., 2016) and hence does not acknowledge the transient effects highlighted by Iverson (1991), Hallet (1996), and Cohen et al. (2006). Results from these steady state treatments suggest that effective pressure exerts a potentially more important control on rates of quarrying than the more well-known influence of sliding speed (Beaud et al., 2014; Ugelvig et al., 2016). However, these studies have tended to consider a relatively high effective pressure, which caused the "volume factor" to dominate and suppress the otherwise potentially important effects of varying differential stress (σ_d) (Ugelvig et al., 2016).

The small-scale glacier bed evolution model of Anderson (2014) again focused attention on the importance of short-term hydrological transients. Anderson (2014) computed the time-dependent evolution of cavities during 5 days of simulated sliding and observed a significant increase in differential stress when water pressure in the cavities drops. The stress thus peaks because of the imbalance between cavity size and water pressure—a phenomenon referred to as the "hammer effect" by Anderson (2014). However, the computations were performed for only a few topographic steps, and the mechanical link between temporal variations in deviatoric stress and the rate of quarrying was not addressed (Anderson, 2014). Thus, the influence of transient effects on rates of quarrying across a glacier bed of heterogeneous strength and containing steps of many different sizes has not yet been studied (Figure 1).

Building on the work of Anderson (2014) and Beaud et al. (2014), we model the spatial and temporal evolution of the hydrological system near the terminus of a glacier over the course of a year, while computing rates of abrasion and quarrying. While Beaud et al. (2014) used a flow-band model, we use a two-dimensional finite element model (FEM) to study the spatial patterns of subglacial erosion that arise due to reorganization of the drainage system. Our subglacial hydrological drainage model closely follows that used by Werder et al. (2013), wherein slow and distributed drainage through cavities coexists with efficient channelized drainage. Bedrock step heights (h) and step lengths (L_s) are randomly distributed, and the associated cavity lengths (S) and channel cross sections (A_c) evolve through time, which allow us to explore how temporal shifts between the competing effects of contact area and differential bedrock stress (equation (1)) influence rates of quarrying. We also use the temporal evolution of the contact area between ice and bedrock ($L_s - S$) to predict how the sizes of cavities influence rates of basal sliding, as well as abrasion by debris moving across the parts of the bedrock in contact with ice (Hallet, 1979). Thus, based on the temporal changes of subglacial hydrology, we strive to integrate, as consistently as possible, the effects of subglacial cavities on sliding speed and on erosion by quarrying and abrasion.

The main objective of our study is to examine how glacial hydrology influences patterns and rates of subglacial erosion. This objective requires that our hydrological model be capable of reproducing the first-order seasonal and diurnal variations of effective pressure as observed in temperate glaciers (Anderson et al., 2004; Bartholomaus et al., 2008; Iken & Bindschadler, 1986; MacGregor et al., 2005). Our focus is especially on the influence of the time-varying ice-bed contact area ($L_s - S$) and temporal pressure variations, which both exert a strong control on sliding speed and subglacial erosion rates.

2. Computational Experiments

The flow of subglacial water is simulated using a two-dimensional FEM. The computational FEM grid is irregular and consists of linear triangular elements (Figure 2a), with bed elevation, $b(x,y)$, and ice thickness, $H(x,y)$, specified in the corner nodes of the triangles. A two-dimensional power law fractal model defines the bed elevation, in which a topographic wavelength, λ, and a Hurst exponent, ν, characterize the bed roughness (Zahouani et al., 1998). The spatial distributions of fractures that are instrumental in controlling bed roughness need not, of course, be fractal, but the simplicity of this assumption and its appropriateness for some rocks (e.g., Aguilar-Hernández & Ramírez-Santiago, 2010; Velde et al., 1991) make this a reasonable starting point. The resulting bed topography (Figure 2) has random variations on many spatial scales and with amplitudes of up to 20 m. Each FEM element is assigned a bed step-length, L_s, from a random fractal distribution between 1 and 30 m (Figure 2d). The step height perpendicular to the ice flow, $h = L_s S_b$, of each element is then computed from the local bed slope S_b (Figure 2e) in the ice flow direction. The latter is calculated in each element from the variation of the element's three nodal elevations. We note that the local bed slope may be opposite the direction of the mean bed slope, in which case the negative step height represents a reverse step. The ice surface profile is approximated by a tilted error function, such that the ice thickness generally increases from zero at $x = 0$ km to 400 m at $x = 3$ km (Figure 2). The ice surface at 3 km then parallels the mean slope of the bedrock landscape. Below we describe the governing equations for subglacial drainage, ice sliding, and subglacial erosion by abrasion and quarrying.

2.1. Subglacial Hydrology

In every time step of a simulation, we compute the distribution of the hydrological head, Ψ, from the following conservation law:

$$\frac{\partial h_w}{\partial t} = -\nabla \cdot \vec{q}_w + \dot{m} \tag{2}$$

where h_w is local water storage, t is time, $\vec{q}_w$ is water flux, and $\dot{m}$ is local water input rate. The water flux relates to the gradient of the hydrological head, ψ, through a Darcy-Weisbach law that is designed to capture simultaneous flow through cavities and channels:

$$\vec{q}_w = -K_w \nabla \psi \tag{3}$$

where

$$K_w = \frac{c_t A_c{}^{\alpha}}{L_c \sqrt{\nabla \psi}} + \frac{c_t A_s{}^{\alpha}}{L_s \sqrt{\nabla \psi}} \tag{4}$$

Here K_W is the effective conductivity, the sum of conductivity though channels (first term) and cavities (second term). The constants c_t and α (Table 1) relate to the Darcy-Weisbach friction factor for turbulent flow, and the combination of the two controls the conductivity of the channel and cavity conduits (Schoof, 2010); A_c and A_s are cross-sectional areas of channels and cavities, respectively; L_c is the characteristic channel width, and L_s is the local cavity spacing perpendicular to water flow (equal to the local step length). These two length scales are used to compute the water discharge in channels and cavities from the water flux in a grid element, that is, $Q_c = L_c q_w$ and $Q_s = L_s q_w$. This assumption implies that if L_s or L_c is below grid resolution, several channels or cavities are assumed to carry the full discharge of the grid element.

The effective pressure, N, is defined to be

$$N = P_i - P_w \tag{5}$$

where

$$P_i = \rho_i g H \tag{6}$$

is the ice overburden pressure and

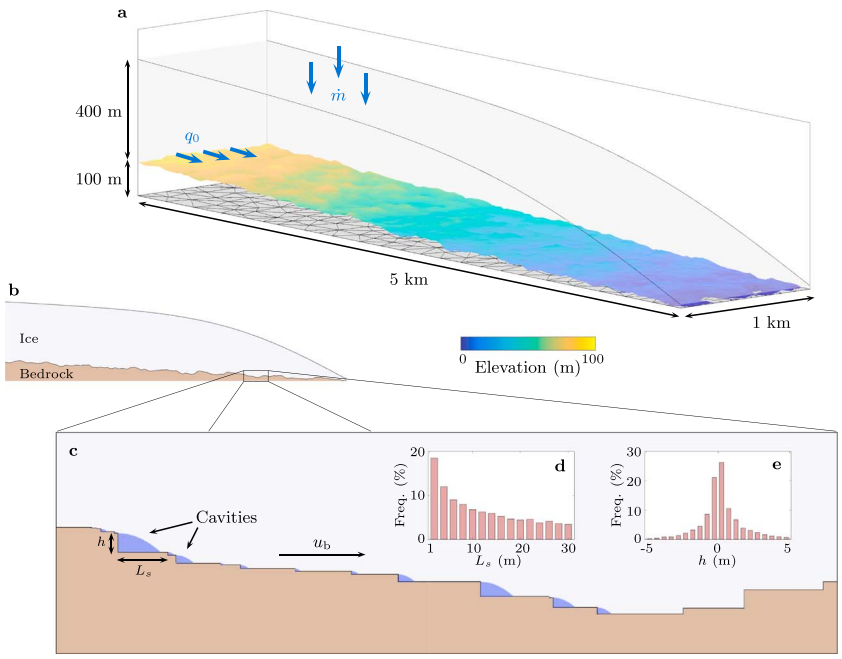

Figure 2. Conceptual sketch of the computational model setup. (a) The geometry of the model and the finite element model mesh. Note that the resolution of the mesh has been greatly reduced for clarity. (b) Longitudinal profile of the model. The mean bed slope is 5%, and the maximum ice thickness is 400 m. (c) Details of staircase bed topography. (d) The fractal distribution of step lengths. (e) The distribution of step heights, which are set by the local bed slope and the step length. Reverse steps have negative step heights.

$$P_w = \psi - \rho_w g b \tag{7}$$

is the subglacial water pressure; ρ_w is the density of water, ρ_i is the density of ice, and g is the acceleration due to gravity.

Channel cross-sectional area is modeled using (Anderson, 2014; Schoof, 2010)

$$\frac{\partial A_c}{\partial t} = \frac{L_c q_w}{\rho_i L_i} \nabla \psi - 2\left(\frac{N}{nB}\right)^n A_c \tag{8}$$

where L_i is the latent heat of fusion of ice and B and n are ice creep parameters (e.g., Hooke, 2005; Table 1). Opening of channels is driven by ice melting due to viscous dissipation of heat from the moving water (first term), while creep of ice acts to close the channels (second term). While the term representing closure depends upon the chosen shape of the channel cross section (e.g., with flatter roof than semicircular), this formulation is conservative in that it results in faster closure by tens of percent (Hooke et al., 1990). A similar balance equation, which stems from Kamb's (1987) analysis of basal cavities, accounts for the temporal evolution of cavity cross-sectional area (Iverson, 2012; Iverson & Petersen, 2011; Ugelvig et al., 2016):

$$\frac{\partial A_s}{\partial t} = u_b h_n - \frac{\pi}{8}\left(\frac{N}{B}\right) S^2 \tag{9}$$

Here u_b is sliding speed, h_n represents "normal" (positive) bedrock steps, and S is cavity length. Cavity length relates to cross-sectional area through $A_s = S h_n \beta$, where β is a dimensionless parameter between 0 and 1 ($\beta = 0.5$ for a linear cavity roof, whereas $0.5 < \beta < 1$ for a convex roof). We follow Anderson (2014) in using $\beta = 0.7$. For cavities, the opening term is considered to be controlled only by sliding over topographic steps (first term); opening due to melting is neglected. This is a reasonable assumption because the discharge through individual cavities and resulting heat dissipation are relatively small (Anderson, 2014; Ugelvig et al., 2016; Walder, 1986). Like the channels, cavities close by ice creep (second term). However, owing to

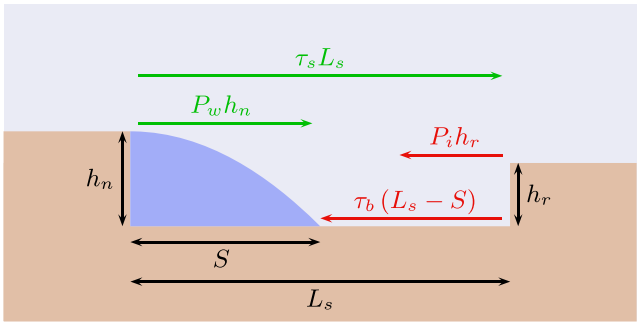

Figure 3. Force balance across a step in the glacier bed. Over the step length, L_s, the horizontal shear stress from the ice, τ_s, acts in the horizontal down-glacier direction with magnitude $\tau_s L_s$. Water pressure, P_w, pushing against the roof of cavities in the lee of normal steps, h_n, contributes with a force $P_w h_n$ in the same direction. Drag from the ice-bed contact area results in a force $\tau_b(L_s - S)$ in the up-glacier direction. Also acting in the up-glacier direction is the force $P_i h_r$ arising from the pressure of ice against reverse steps, h_r.

the high aspect ratios of cavities, their closing rates scale with cavity length squared rather than cross-sectional area (Iverson, 2012; Iverson & Petersen, 2011; Kamb, 1987).

Finally, in order to close equation (2) we assume that water storage, h_w, occurs in cavities and channels, as well as in an englacial aquifer with void ratio e_G (Table 1). The englacial storage mechanism is necessary to explain delays between daily maximum meltwater input and output from glaciers (Bartholomaus et al., 2011). We follow Werder et al. (2013) in assuming that the volume of stored englacial water scales linearly with water pressure:

$$h_w = \frac{A_s}{L_s} + \frac{A_c}{L_c} + e_G \frac{P_w}{\rho_w g} \tag{10}$$

Here the three terms on the right-hand side describe water storage in cavities, channels, and englacial voids, respectively.

As boundary conditions to the hydrological model, zero flow is enforced at the two parallel interior boundaries, while water flux into the model domain from areas up-glacier, q_0, is specified at the upper boundary (Figure 2). This base flux scales linearly with the ice-surface melt rate, $q_0 = k_0\dot{m}$, except when the surface melt-rate is zero during winter or cold nights (Table 1). At these times q_0 is assigned a low constant value, $q_0 = 0.001$ m^2 s^{-1}, to account for the small englacial and subglacial melt production by frictional and geothermal heating. Zero water pressure is imposed at the lower grid boundary, corresponding to air pressure at the ice margin. At the ice surface, we specify a uniformly distributed but temporally varying melt rate. The surface melt rate is varied through time to mimic yearly-to-daily variations in mass balance. We do not model any superglacial or englacial flow, and we therefore assume that the surface melt immediately enters the subglacial hydrological system. This is appropriate as long as the moulins or crevasses that serve as connections between surface and deep flow systems are relatively closely spaced.

2.2. Basal Sliding

We use a simple horizontal force balance in the stair-case subglacial setting (Figure 3) to formulate a sliding law that includes effects from both cavities and water pressure. The force balance is inspired mainly by the work of Iken (1981). Overall, sliding of the ice is driven by a basal shear stress, which may equal the driving stress or may include contributions from horizontal longitudinal and transverse stress components. We assume that the horizontal component of the shear stress, τ_s, is the average driving stress of the modeled ice volume (Table 1), which corresponds to a situation in which horizontal coupling is strong enough to counteract all gradients in stress and sliding speed across the model domain. Hence, we do not model ice dynamics apart from predicting the average sliding rate though time. We furthermore assume that sliding speed decreases to zero at the ice margin, following the same error function that controls ice thickness (Figure 2).

Over the step length, L_s, the uniform shear stress contributes with a down-glacier horizontal force of magnitude $\tau_s L_s$. Acting in the same direction is a force generated by water pressure against the cavity roof (Iken, 1981). Integrating the horizontal component of the water pressure, we find the latter force to be $P_w h_n$ regardless of the form of the cavity roof. Here h_n represents positive (normal) steps. Opposing these two down-glacier directed forces are two horizontal forces acting up-glacier. The first, $P_i h_r$, is caused by the ice pressing against reverse steps ($h_r < 0$), and the second, $\tau_b(L_s - S)$, comes from basal drag along the ice-bed contact area. We assume that the basal drag equals the viscous stress associated with ice creep along the contact area. Using Glen's flow law:

$$\tau_b = K_s {u_b}^{1/n} \tag{11}$$

where K_s is a creep-sliding parameter. In applying this relationship to the flat treads of steps, we assume implicitly that these surfaces have roughness at scales less than L_s that will provide form drag. We note, however, that the basal drag could also include contributions from friction between bedrock and debris in the basal ice

(e.g., Iverson et al., 2003), although we do not include such contributions here. Averaging the force balance across the model domain and rearranging equation (11) yields the following sliding law:

$$u_b = \left[\frac{1}{K_s \overline{F_c}}\left(\tau_s + \frac{\overline{P_w h_n}}{L_s} + \frac{\overline{P_i h_r}}{L_s}\right)\right]^n \tag{12}$$

where $F_c = (1 - S/L_s)$ is the local ice-bed contact ratio. The horizontal bars represent model-domain averaging. Note that the last term on the right-hand side of equation (12) is negative due to the sign of the reverse steps ($h_r < 0$).

We note that the sliding law above allows water pressure to influence sliding speed in two ways. First, the push from water in cavities ($P_w h_n$) can vary rapidly as water pressure fluctuates, for example, in response to variations in surface melt input. Second, water pressure influences sliding by controlling the average ice-bed contact ratio $\overline{F_c}$; this effect works more slowly, as described by equation (9) and sliding hence remains stable even for $P_w > P_i$, as long as $\overline{F_c} > 0$.

Moreover, the sliding law fulfills two important characteristics highlighted by Schoof (2005) for cavity-based sliding laws: (i) The sliding law approaches a Weertman-type sliding law for small cavities ($\overline{F_c} \simeq 1$ and $\overline{P_w} \simeq 0$), in which sliding speed becomes a nonlinear function of shear stress but not of effective pressure; (ii) the bed-averaged basal drag, $\overline{\tau_b F_c}$, reaches an asymptotic upper limit if sliding speed continues to rise because as u_b rises, F_c decreases due to the influence of sliding on cavity length (equation (9)) (Gagliardini et al., 2007; Iken, 1981; Schoof, 2005). Through these characteristics, the sliding law allows direct parameterization of bed roughness in a stair-case topographic setting. We argue that it realistically captures important feedbacks among cavitation, ice-bed contact area, and basal sliding.

2.3. Subglacial Erosion

Based on the temporal evolution of sliding, effective pressure, and ice-bed contact area, we model the rates of erosion though time. Given the short time scale of the experiments (a few years) and hence limited total erosion, we do not, however, adjust the bed topography in response to this erosion. For the same reason, we assume that sediment produced at the bed is removed immediately and does not protect the bed from further erosion.

2.3.1. Abrasion

Abrasion is modeled by adopting Hallet's abrasion law (Hallet, 1979), in which abrasion rate, E_a, scales as sliding rate squared. This abrasion law builds on the argument that for a rough bed in contact with ice both the flux of debris particles in the basal ice and the contact force between debris particles and the bed scale approximately linearly with the sliding speed (Hallet, 1979). We again assume implicitly that treads between steps have roughness. In addition, we use the effective ice-bed contact ratio F_c to account for cavities where no abrasion occurs:

$$\dot{E}_a = K_a F_c u_b^2 \tag{13}$$

The scaling constant K_a depends on basal-ice debris concentration, debris-particle shape, and the relative hardness of debris particles and bedrock (Hallet, 1979). We do not model variation in these properties here and hence treat K_a as a constant. As noted, friction associated with abrasive debris is assumed to be sufficiently small to be neglected in the force balance (equation (12)).

2.3.2. Quarrying

Rates of quarrying are computed from the theory of Iverson (2012):

$$\dot{E}_q = \frac{F_c u_b h_n k}{2L_s} \tag{14}$$

Here k is the aforementioned probability of erosion of a normal (positive) topographic step characterized by height h_n and length L_s (equation (1)). The model for quarrying rate (equation (14)) builds on the assumption that every quarrying event removes half of the bedrock step in contact with the ice (a block of dimension

$h_n \times L_s$; Iverson, 2012). In order to compute k, we first find the differential stress, σ_d, in the bedrock (Hallet, 1996; Iverson, 2012) by

$$\sigma_d = \begin{cases} c(\sigma_n - P_w) = \dfrac{cN}{F_c} & \text{for} \quad \sigma_n - P_w < \sigma_n^* \\ c\sigma_n^* & \text{for} \quad \sigma_n - P_w \geq \sigma_n^* \end{cases} \tag{15}$$

Here σ_n is the stress oriented normal to the bed, c is a scaling factor, and σ_n^* represents the brittle yield stress of ice (Table 1). We take the Weibull modulus, m, contributing to the quarrying likelihood k (equation (1)), to be 3 in our experiments, which is within the range of values, 1.5–5, considered by Iverson (2012). The probability of quarrying of a step, k, is determined both by the size of the rock volume in contact with the ice ("volume factor") and the differential stress ("differential stress factor"). The higher the value of m, the more weight is assigned to the importance of differential stress in determining k and less to the volume factor (equation (1)). This means that erosion is generally faster for lower values of m because then the volume factor dominates and k is high on large steps (equation (1)). However, although not studied here, we note that in situations in which the bedrock is dissected by a distinct joint set, the joint spacing may exert a stronger control on the quarried volume than the contact area between ice and bedrock (Dühnforth et al., 2010; Hooyer et al., 2012).

3. Results

Below we present results from experiments in which we explore the influence of variations in meltwater input on the spatial and temporal patterns of subglacial erosion. We focus first on yearly variations in which meltwater varies due to seasonality. We next include the influence of shorter-term variations, that is, monthly, weekly, and daily, incorporating meltwater variability due to weather in the first two cases and diurnal cycles in the latter.

3.1. Experiment 1: Yearly Variations

We mimic seasonal meltwater input as a truncated sinusoidal function with a period of 1 year (Figure 4d). Starting in winter, the ice surface temperature is assumed to be below 0 °C, and there is no input of surface meltwater. Still, the hydrological system receives water from the base flux, q_0, as noted. Due to the low flux of water (Figure 4d, day 50), the subglacial hydrological system first operates at low capacity, with relatively small conduits in cavities and channels (Figures 4a and 4d). The ice-bed contact ratio is high (~0.95), and sliding is hence relatively slow (~50 m yr^{-1}, Figure 4f). The inefficient drainage system generally keeps water pressure high and effective pressure relatively low (~1 MPa) in spite of the modest water input (Figure 4g). In this period the bed experiences moderate levels of differential stress (Figure 4h) and moderate rates of quarrying (Figure 4i), whereas rates of abrasion are low (Figure 4i) due to the slow sliding.

The melt rate at the glacier surface starts to increase in early spring, and water input to the bed quickly exceeds the capability of the hydrological system to transport the water (Figure 4d, around day 90). This results in a drop of average effective pressure to ~0.2 MPa, corresponding to 10% of the ice overburden pressure (Figure 4g). The decrease of effective pressure allows cavities to grow larger, reducing both the ice-bed contact area (Figure 4e) and the basal drag. The reduced contact area thus increases sliding speed, which is further enhanced by the high water pressure in the cavities that "pushes" the glacier forward (Figure 4f). The pronounced increase of sliding speed in spring (Figure 4f, day 90 to 120) is a common phenomenon (often referred to as the "spring event" (Röthlisberger & Lang, 1987)) observed in the surface velocity of both alpine and outlet glaciers and hence provides support for our cavity-based sliding law (Anderson et al., 2004; Bartholomaus et al., 2008, 2011; Iken & Bindschadler, 1986; Iken & Truffer, 1997; MacGregor et al., 2005; Müller & Iken, 1973). For example, over the course of a month, Bartholomaus et al. (2008, 2011) reported increases in surface velocities of up to 200% above winter velocities, followed by a period of decreasing velocities in the late summer months. Our cavity-based sliding law fully reproduces such behavior.

The "spring event" has a profound impact on rates of abrasion and quarrying (Figures 4b and 4c, middle panels). Abrasion is clearly enhanced by the increase in sliding speed, and rates of abrasion consequently peak in late spring when sliding speed exceeds 300 m yr^{-1} (Figures 4f and 4i). In contrast, the average rate

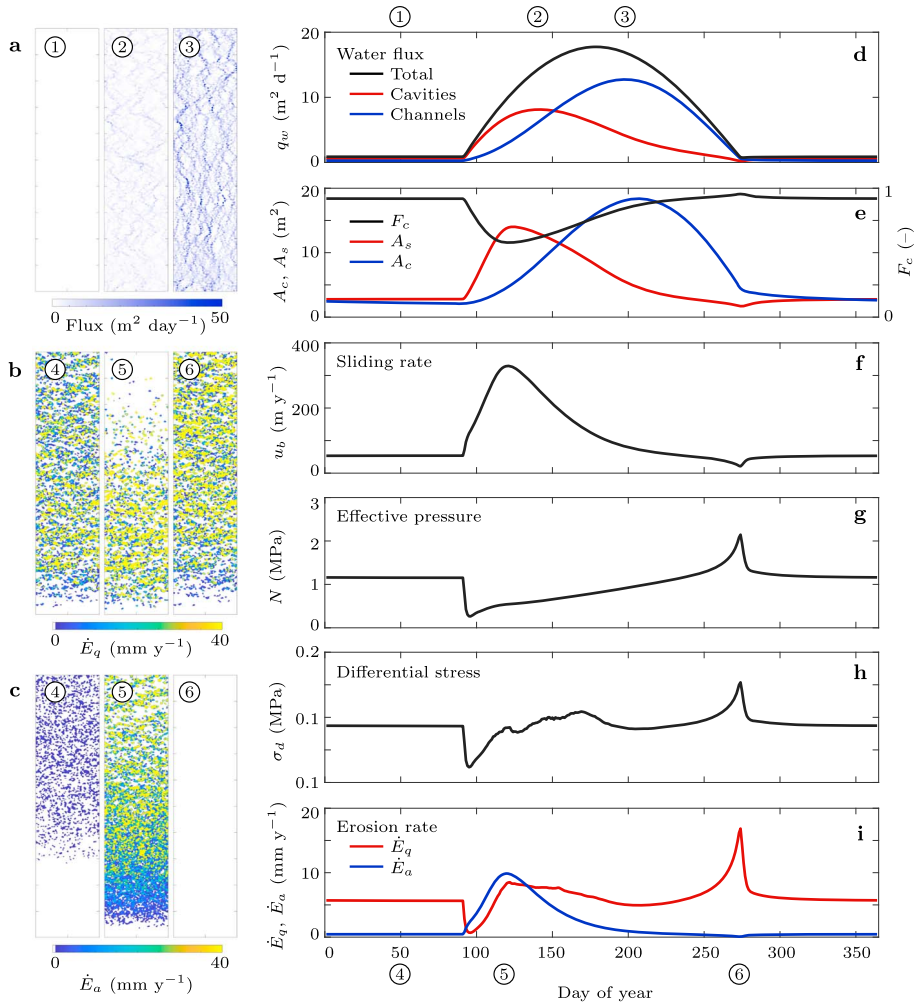

Figure 4. Results from experiment 1 with seasonal melt variation. Spatial patterns of (a) water flux, (b) rates of quarrying, and (c) rates of abrasion at three different times marked by numbered circles in (d) and (i). (a)–(c) are maps of the glacier bed seen from above. The direction of ice and water slow is from top to bottom. Also shown is the temporal evolution of (d) mean water flux in cavities and channels, (e) ice-bed contact ratio (F_c) and mean cross-sectional area of cavities (A_s) and channels (A_c), (f) sliding speed, (g) effective pressure, (h) differential stress, and (i) normalized rates of quarrying ($\dot{E}_q$) and abrasion ($\dot{E}_a$).

of quarrying decreases in early spring (Figure 4i), mainly in response to the higher water pressure in cavities, which decreases the average differential stress (Figure 4h), particularly in the upper parts of the model domain (Figure 4b, middle).

By the time the surface melt rate peaks in midsummer, the subglacial system has adapted to the increased water flux and channels now handle most of the meltwater discharge (Figure 4a, right and Figure 4e). As the channels gradually develop in summer, cavities start to shrink and the ice-bed contact area slowly grows, thereby slowing sliding (Figures 4e and 4f). However, before the cavities fully collapse to their winter configuration, the relatively high effective pressure and low ice-bed contact area of the summer combines to maximize the ice-bed contact ratio and the differential bedrock stress (Figures 4e and 4g), which accelerates quarrying (Figure 4i). Quarrying is now active also the upper part of the domain, where meltwater channelization has increased the contact area between ice and bed just enough for the differential stress to show its influence (Figure 4b, right).

The rate of quarrying is generally controlled by variations in differential stress, which depend both on the contact area ($L_s - S$) and the water pressure within cavities (equations (1) and (14)). As a consequence the

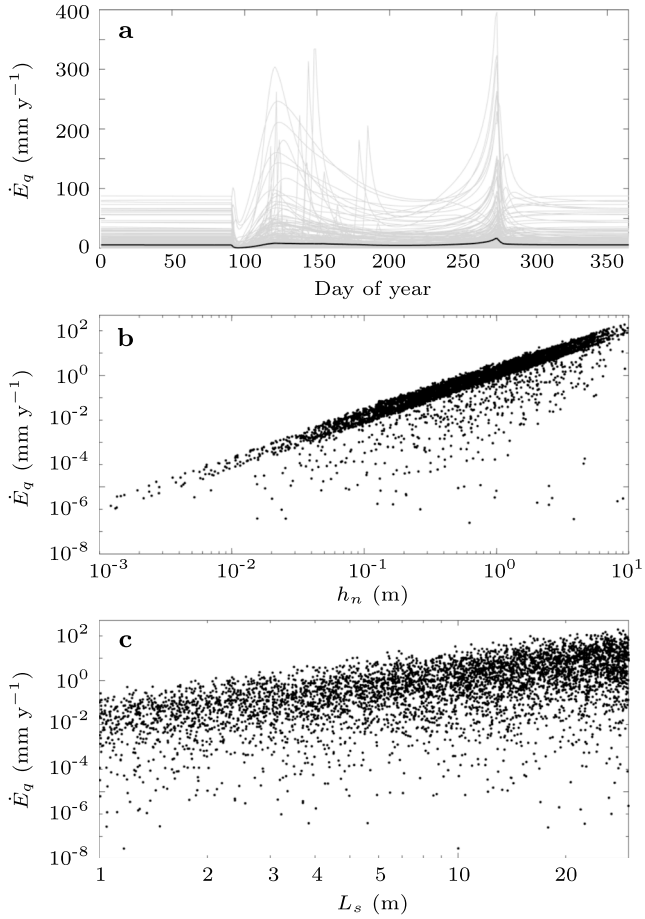

Figure 5. Variation of quarrying between topographic steps during seasonal melt variation. (a) Quarrying rates from 1% of the steps are shown as gray lines. The 1% steps were randomly selected. The solid black line is the quarrying rate averaged for all steps. (b) Yearly averaged quarrying rate as function of step height, h_n. (c) Yearly averaged quarrying rate as function of step length, L_s.

rate of quarrying varies hugely among bedrock steps (Figure 5). In a situation where a particular step becomes drowned by a cavity, differential stress peaks just before and just after complete drowning. Only a very small contact area then supports the load of the ice, and this amplifies the contact stress to levels more than 5 times the ice overburden pressure. This results in sudden pulses of efficient quarrying at many topographic steps (Figure 5a, gray lines). However, due to the variation in step length, L_s, and step height, h_n, the quarrying pulses do not occur simultaneously for the different steps. Moreover, the few large topographic steps, with large step heights or step lengths, cause orders-of-magnitude faster quarrying than the many smaller steps (Figures 5b and 5c), which is why the averaged quarrying rate shows a smaller peak than the fastest eroding steps (Figures 4i and 5a).

Overall, ice-bed contact area is a key variable in controlling both sliding speed and rates of erosion in this yearly experiment. However, higher-frequency fluctuations in water pressure and sliding speed also play an important role (Anderson et al., 2004; Bartholomaus et al., 2008, 2011; Iken & Bindschadler, 1986), as illustrated by the next experiment.

3.2. Experiment 2: The Influence of Time Scale

In order to explore how the period of variation in meltwater production influences erosion, we perform a series of four experiments in which meltwater production is controlled by the same sinusoidal variation, but with periods of a year, a month, a week, and a day, respectively (Figure 6). In each experiment, the meltwater production varies from 0 to 10 cm d^{-1} around a mean of 5 cm d^{-1}. For comparison, we also show a simulation with steady melt production at 5 cm d^{-1}.

The experiments show how the average ice-bed contact area varies less when the period of variation is shortened from a year to months, weeks, and days (Figure 6b). While the yearly and monthly variations in meltwater production reduce the contact area periodically from 95% to 75%, weekly variations reduce the contact ratio by only ~5% and daily variations by less than 2%. The variability of the contact area is smaller for short-term periods because the time available to grow cavities by sliding and shrink them by creep is shorter, and hence, the cavity system has less time to react to the forcing provided by water flux (equation (9)). Consequently, the variability in average effective pressure (Figure 6c) is generally larger for short-term variations because cavities and channels are undersized during periods of high water flux (requiring high water pressure) and oversized in periods of low water flux (allowing water to flow at low pressure). The daily variation (Figure 6c, blue curve) is an exception to this pattern, however; in this case water storage in the englacial void system (equation (10)) delays and smoothens the variability in subglacial water flux during the day. Hence, the daily variability in effective pressure is smaller than the corresponding weekly variability. The sliding rate (Figure 6d) is primarily influenced by the average contact ratio, and hence, it varies strongly for the yearly and monthly periods and much less for the weekly and daily simulations when changes in water pressure rather than contact ratio control sliding (equation (12)). We note, however, that sliding rates still vary considerably in the short-term simulations (50–200 m yr^{-1} for the weekly period and 100–150 m yr^{-1} for the daily period), but the maximum rate (150 m yr^{-1}) is much smaller than the rate achieved in the yearly (~300 m yr^{-1}) and monthly (~350 m yr^{-1}) simulations.

The large variation in effective pressure transfers almost directly to rates of quarrying (Figure 6e), particularly for the intermediate periods (months and weeks). During the low-melt phases of the weekly simulation, average rates of quarrying reach 20 mm yr^{-1}, which is more than 5 times faster than the constant quarrying rate in the steady simulation without meltwater variability. On the other hand, abrasion is in our experiments

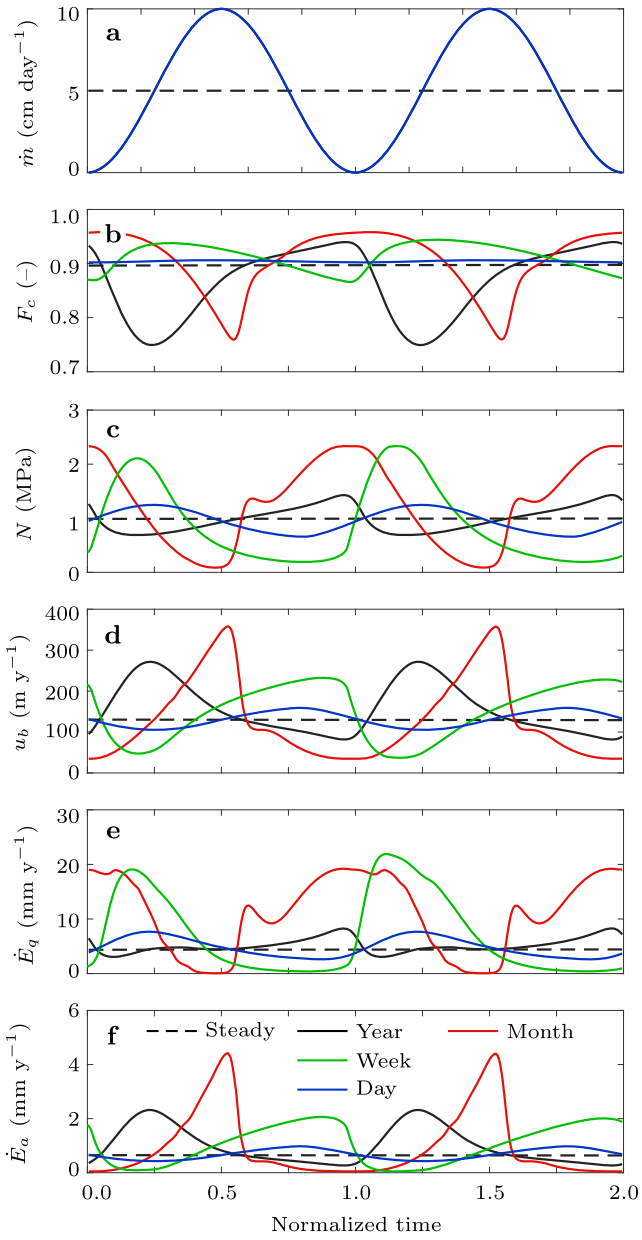

Figure 6. Results from experiment 2 using yearly, monthly, weekly, and daily melt-production variations. Time scales (horizontal axes) have been normalized to show two periods in each case. (a) The generic sinusoidal variation in melt production. The dashed line marks the mean production rate, which is used in the steady simulation. (b) Average ice-bed contact ratio through time. (c) Effective pressure. (d) Basal sliding rate. (e) Rate of quarrying. (f) Rate of abrasion.

solely controlled by sliding rate and ice-bed contact ratio and hence varies substantially over yearly to monthly periods and much less over the shorter periods (Figure 6f).

Averaging the rates of erosion over the respective periods, we find that variability in meltwater production consistently accelerates both quarrying and abrasion, especially for weekly and monthly variations in which the time-averaged rate of erosion is several times higher than the rate achieved in the steady simulation (Figure 7). We supplemented the experiment shown in Figure 6 by two other experiments having (i) a less steep bed (2%) and thicker ice (750 m) and (ii) a steeper bed (10%) and thinner ice (150 m). All experiments have the same driving stress as scaled by the product of bed slope and ice thickness. Comparing these three experiments (Figure 7) shows that meltwater variability enhances quarrying the most in the experiment with a flat bed and thick ice, while abrasion is more sensitive to the variations in the steeper bed, thinner ice experiment. The reason for this difference lies in the dependence of the two processes on effective pressure and sliding velocity. Quarrying is most sensitive to variations in effective pressure, which are greatest in the thick-ice experiments, while larger variations in sliding speed boosts abrasion the most in the experiment with the steeper bed.

4. Discussion

4.1. Sliding Speed and Effective Pressure

Basal sliding plays an important role in both subglacial quarrying and abrasion. We note two important situations in which the cavity-based sliding model (equation (12)) differs from a more standard sliding law that depends only on shear stress and effective pressure:

$$u_b = C\frac{{\tau_b}^n}{N} \tag{16}$$

where C is a sliding coefficient.

First, the increase in sliding during spring is typically attributed to meltwater entering a low capacity drainage system. This can result in water pressure increasing, which in turn causes faster sliding (Bartholomaus et al., 2011; Iken & Bindschadler, 1986; Iken & Truffer, 1997). Our model experiments suggest a similar sliding pattern, and simulated sliding speeds increase to 500% above the winter level over a period of approximately 2 months (Figure 4f). Importantly, however, there is an offset between the peak in sliding speed and the drop in effective pressure (Figures 4f and 4g). Using the standard sliding law (equation (16)), the two would be perfectly anticorrelated because of the inverse relation between sliding speed and effective pressure (Anderson, 2014; Beaud et al., 2014). Our cavity-based sliding law, on the other hand, depends on effective pressure primarily through the extent of cavitation (the $(1/F_c)^n$ factor in equation (12)), which shifts the peak in sliding to the time when the average ice-bed contact area is at its minimum (Figure 4e). Second, measurements of effective pressure in winter are often relatively low, in spite of slow sliding (Fleurian et al., 2016; Harper et al., 2005; Iken & Bindschadler, 1986; Lappegard & Kohler, 2005). This is difficult to explain using the standard sliding law above (equation (16)), again because effective pressure and sliding speed are anticorrelated. However, in the cavity-based sliding law, the shrinkage of cavities in winter has two effects: First, it reduces the hydrologic conductivity and keeps water pressures high in spite of low water flux, and second, it slows sliding by increasing the ice-bed contact area and hence the basal drag.

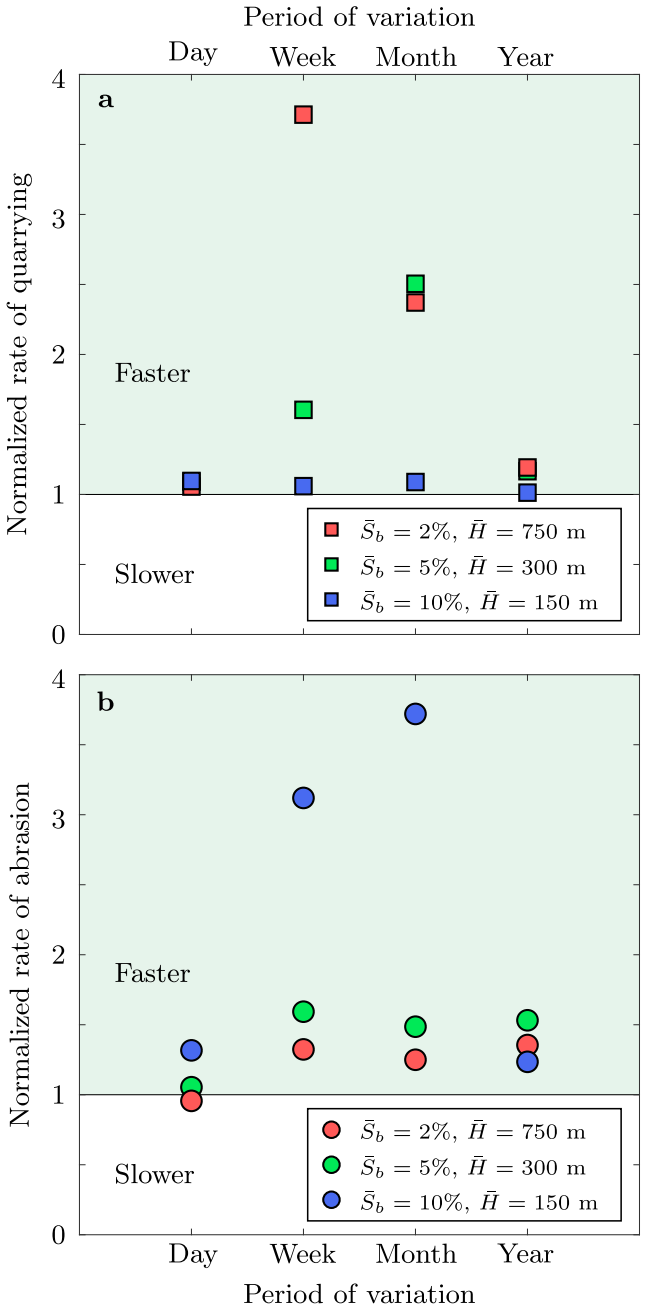

Figure 7. The influence of melt-production variability on average rates of glacial erosion. The rates are normalized by the rate of the corresponding steady simulation. (a) Normalized rates of quarrying. (b) Normalized rates of abrasion. Three models of different combinations of ice thickness and bed slope are shown. The three models have the same driving stress (scaled by bed slope times ice thickness). All models produce the same total melt; only the period of the variation varies.

As sliding speed is thus controlled both by the temporally varying drag exerted by the bed and by water pressure in the cavities, there exists no simple dependence on effective pressure. Furthermore, water storage relates to the size of cavities and to their water pressure (equation (10))—two parameters that have been observed to control sliding speed (Anderson et al., 2004; Hodge, 1974; Iken & Bindschadler, 1986; Kamb et al., 1994; MacGregor et al., 2005). Iken and Bindschadler (1986) found that synchronous variations in water level between different boreholes correlated with horizontal surface velocities and used these observations to argue that water pressure exerts the primary control on sliding speed. Based on considerations of input to and discharge from the basal drainage system, Kamb et al. (1994), on the other hand, argued that horizontal velocities should most directly correlate with the amount of water stored at the bed (Fountain & Walder, 1998), consistent with subsequent measurements at some hard-bedded glaciers (Harper et al., 2007). According to Kamb et al. (1994), sliding speed as well as storage at the bed are dictated by the basal water pressure averaged over the length scale of ice-velocity variations (Fountain & Walder, 1998). Sliding speed is thus expected to correlate with storage, but not necessarily with rapid local water pressure fluctuations (Fountain & Walder, 1998). The length scale at which water pressure should be averaged is estimated to be more than 4 times the ice thickness (Mair et al., 2001), a criterion we meet by averaging the water pressure used in the sliding law across the entire model domain (1 × 5 km).

4.2. The Influence of Hydrologic Variability

Experimental studies have shown that rapid fluctuations in cavity water pressure enhance growth of preexisting fractures in bedrock by periodically increasing the differential stress (Cohen et al., 2006). A sudden drop in water pressure transfers the weight of the ice from the cavity roof to the remaining area of the bed in contact with the ice. This can elevate bed normal stress to several times the ice overburden pressure, especially for large cavities where the ice-bed contact area is relatively small (Anderson, 2014; Hallet, 1996; Iverson, 1991). Our study generally confirms this combined influence of effective pressure and cavity size, sharply increasing rates of quarrying during short periods in which the ice "hammers" the contact area between ice and bedrock (Anderson, 2014). However, due to spatial variation in topography and hence cavity size, this hammer operates at different times across the glacier bed. Rates of quarrying can thus remain high for longer periods when averaged across the bed (Figure 5a). We find that this effect generally causes variability in meltwater delivery to the bed to dramatically accelerate quarrying (Figures 6 and 7). We therefore suggest that this effect contributes to making glaciers at lower latitudes overall more erosive than polar glaciers (Herman & Brandon, 2015; Koppes et al., 2015).

We find weekly-monthly variations in meltwater production to be the most effective in accelerating quarrying in our experiments. Such monthly variations are particularly relevant for temperate regions where synoptic-scale changes in weather conditions influence surface ablation particularly in spring and autumn. The weekly-monthly time scale has the largest impact on quarrying in our experiments because it is (i) slow enough to avoid the dampening effect of englacial storage on water flux, but (ii) fast enough to bring the sizes of cavities and channels out of balance with the water flux. The

reaction time of cavities and channels depends, however, on a number of conditions. For example, the average sliding rate of a glacier determines how quickly cavities can grow in response to an increase in sliding or a decrease in effective pressure. Also, ice thickness limits effective pressure and hence the closing rate of both cavities and channels. For example, Anderson (2014) modeled basal sliding with diurnal amplitudes of approximately 400 m yr^{-1}; this resulted in a faster dynamic system in which cavities grew and shrunk at rates of up to 1 m d^{-1}. As a result, the highest differential stress occurred when water pressure in the cavity was decreasing and the cavity was still covering a large fraction of the bed (i.e., just as the cavity starts to close in response to higher effective pressure). In our experiments with daily water-pressure fluctuations, we also observe pulses of faster quarrying, although at a slightly different time (Figure 6). Since the response time of cavities in our model is significantly longer, primarily due to much smaller variation in diurnal sliding speed, they cannot adjust fast enough to daily fluctuations. The peak in quarrying thus occurs when water pressure is at its minimum (Figures 6c and 6e). This elevates the differential stress and hence the quarrying rate, especially for steps associated with a small ice-bed contact area.

The influence of effective pressure, and pressure variations, also bears on efforts to develop empirical erosion rules for glacial landscape evolution models. Such studies commonly use field observations of sediment discharge in outwash streams of glaciers as a proxy for erosion rate (assuming that eroded bedrock is immediately released to streams) and consider control variables that are easily measured, such as glacier velocity, while neglecting other variables, such as effective pressure (e.g., Herman et al., 2015). In this study we have illustrated how neglect of effective pressure may under-represent the influence of quarrying, particularly at the long time scales most relevant to landscape evolution models.

4.3. Coupling of Abrasion and Quarrying

In this study quarrying and abrasion are modeled as independent processes. However, they are in fact highly coupled processes because quarrying produces the debris that drives abrasion (Hallet, 1979). The pace of abrasion, therefore, depends not only on sliding speed and contact area but also on the availability of debris in the basal ice. The timing of abrasion may therefore be influenced by temporal and spatial patterns of quarrying, possibly shifting the peak in abrasion to later in the year when sliding speed is below the maximum level reached in spring (Figure 4). On the other hand, previous periods of efficient quarrying may have generated enough debris to keep rates of abrasion high, also during periods of inefficient quarrying. Our assumption of constant K_a in equation (13) is based on this situation. Finally, rates of debris production by both quarrying and abrasion can exceed rates of debris transport, resulting locally in till layers that separate ice from rock and protect it from erosion. These kinds of effects represent complex feedbacks between erosion rates and glaciological variables. However, capturing such feedbacks would require modeling of debris transport and comminution (MacGregor et al., 2009; Ugelvig & Egholm, 2018), which is outside the scope of the present contribution.

5. Conclusions

We have presented a two-dimensional model for subglacial water drainage coupled to erosion models for abrasion and quarrying. Importantly, as our cavity-based sliding law can reproduce first-order seasonal patterns in sliding speed observed on temperate glaciers, it may better capture the basal conditions that drive subglacial erosion than sliding laws used in previous erosion models. We have explored how rates of subglacial erosion are influenced by drainage reorganization due to yearly-to-daily variations of surface meltwater input to the bed. On yearly time scales the effective contact area between ice and bed strongly controls rates of erosion by both scaling the differential stress in the bedrock (important for quarrying) and influencing sliding speed (important for abrasion). Rates of abrasion thus peak in spring when sliding is accelerated by high water pressure and the growth of cavities. In contrast, rates of quarrying peak in autumn as the cavity-channel system of the summer returns to low capacity. Shorter-term variations (monthly, weekly, and daily) of the melt rate generally accelerate quarrying by forcing the subglacial drainage system to be out of sync with the water flux, which in turn modulates water pressure and cavity size. This increases effective pressure in short intervals of time and overall leads to faster quarrying. In summary, we have demonstrated the great importance of variations in the hydrologic system that serve to drive complex variations in sliding speed, cavity length, and water pressure. These variations combine to produce conditions conducive to quarrying and abrasion at different times beneath glaciers.

Acknowledgments

The authors thank Roger LeB. Hooke and Bryn Hubbard for valuable reviews that improved the manuscript. This study was supported by Independent Research Fund Denmark (grant DFF-6108-00226) and a mobility grant from Aarhus University Research Foundation to DLE. RSA acknowledges support from the National Science Foundation grant EAR-1548725. The computational MATLAB codes are available as supporting information.

References

Aguilar-Hernández, A., & Ramírez-Santiago, G. (2010). Self-similar and self-affine properties of two-dimensional fracture patterns in rocks. *Mathematical Geoscience*, *42*(8), 925–954. https://doi.org/10.1007/s11004-010-9279-4

Anderson, R. S. (2014). Evolution of lumpy glacial landscapes. *Geology*, *42*(8), 679–682. https://doi.org/10.1130/G35537.1

Anderson, R. S., Anderson, S. P., MacGregor, K. R., Waddington, E. D., O'Neel, S., Riihimaki, C. A., & Loso, M. G. (2004). Strong feedbacks between hydrology and sliding of a small alpine glacier. *Journal of Geophysical Research*, *109*, F01020. https://doi.org/10.1029/20051F000359

Anderson, R. S., Molnar, P., & Kessler, M. A. (2006). Features of glacial valley profiles simply explained. *Journal of Geophysical Research*, *111*, F01004. https://doi.org/10.1029/2005JF000344

Bartholomaus, T. C., Anderson, R. S., & Anderson, S. P. (2008). Response of glacier basal motion to transient water storage. *Nature Geoscience*, *1*(1), 33–37. https://doi.org/10.1038/ngeo.2007.52

Bartholomaus, T. C., Anderson, R. S., & Anderson, S. P. (2011). Growth and collapse of the distributed subglacial hydrologic system of Kennicott glacier, Alaska, USA, and its effects on basal motion. *Journal of Glaciology*, *57*(206), 985–1002. https://doi.org/10.3189/002214311798843269

Beaud, F., Flowers, G. E., & Pimentel, S. (2014). Seasonal-scale abrasion and quarrying patterns from a two-dimensional ice-flow model coupled to distributed and channelized subglacial drainage. *Geomorphology*, *219*, 176–191. https://doi.org/10.1016/j.geomorph.2014.04.036

Becker, R. A., Tikoff, B., Riley, P. R., & Iverson, N. R. (2014). Preexisting fractures and the formation of an iconic American landscape: Tuolumne meadows, Yosemite National Park, USA. *GSA Today*, *24*(11), 4–10. https://doi.org/10.1130/GSATG203A.1

Cohen, D., Hooyer, T., Iverson, N., Thomason, J., & Jackson, M. (2006). Role of transient water pressure in quarrying: A subglacial experiment using acoustic emissions. *Journal of Geophysical Research*, *111*, F03006. https://doi.org/10.1029/2005JF000439

De Fleurian, B., Gagliardini, O., Zwinger, T., Durand, G., Le Meur, E., Mair, D., & Raback, P. (2014). A double continuum hydrological model for glacier applications. *The Cryosphere*, *8*(1), 137–153. https://doi.org/10.5194/tc-8-137-2014

Dühnforth, M., Anderson, R. S., Ward, D., & Stock, G. M. (2010). Bedrock fracture control of glacial erosion processes and rates. *Geology*, *38*(5), 423–426. https://doi.org/10.1130/G30576.1

Egholm, D. L., Jansen, J. D., Brædstrup, C. F., Pedersen, V. K., Andersen, J. L., Ugelvig, S. V., et al. (2017). Formation of plateau landscapes on glaciated continental margins. *Nature Geoscience*, *10*(8), 592–597. https://doi.org/10.1038/ngeo2980

Egholm, D. L., Nielsen, S. B., Pedersen, V. K., & Lesemann, J.-E. (2009). Glacial effects limiting mountain height. *Nature*, *460*(7257), 884–887. https://doi.org/10.1038/nature08263

Egholm, D. L., Pedersen, V. K., Knudsen, M. F., & Larsen, N. K. (2012). On the importance of higher order ice dynamics for glacial landscape evolution. *Geomorphology*, *141-142*, 67–80. https://doi.org/10.1016/j.geomorph.2011.12.020

Fleurian, B., Morlighem, M., Seroussi, H., Rignot, E., van den Broeke, M. R., Munneke, P. K., et al. (2016). A modeling study of the effect of runoff variability on the effective pressure beneath Russell glacier, west Greenland. *Journal of Geophysical Research: Earth Surface*, *121*, 1834–1848. https://doi.org/10.1002/2016JF003842

Flowers, G. E., & Clarke, G. K. (2002). A multicomponent coupled model of glacier hydrology 1. Theory and synthetic examples. *Journal of Geophysical Research*, *107*(B11), 2287. https://doi.org/10.1029/2001JB001122

Fountain, A. G., & Walder, J. S. (1998). Water flow through temperate glaciers. *Reviews of Geophysics*, *36*, 299–328. https://doi.org/10.1029/97RG03579

Gagliardini, O., Cohen, D., Råback, P., & Zwinger, T. (2007). Finite-element modeling of subglacial cavities and related friction law. *Journal of Geophysical Research*, *112*, F02027. https://doi.org/10.1029/2006JF000576

Hallet, B. (1979). A theoretical model of glacial abrasion. *Journal of Glaciology*, *23*, 39–50.

Hallet, B. (1996). Glacial quarrying: A simple theoretical model. *Annals of Glaciology*, *22*, 1–8. https://doi.org/10.1017/S0260305500015147

Harper, J. T., Humphrey, N. F., Pfeffer, W. T., Fudge, T., & O'Neel, S. (2005). Evolution of subglacial water pressure along a glacier's length. *Annals of Glaciology*, *40*(1), 31–36. https://doi.org/10.3189/172756405781813573

Harper, J. T., Humphrey, N. F., Pfeffer, W. T., & Lazar, B. (2007). Two modes of accelerated glacier sliding related to water. *Geophysical Research Letters*, *34*, L12503. https://doi.org/10.1029/2007GL030233

Herman, F., Beaud, F., Champagnac, J.-D., Lemieux, J.-M., & Sternai, P. (2011). Glacial hydrology and erosion patterns: A mechanism for carving glacial valleys. *Earth and Planetary Science Letters*, *310*(3-4), 498–508. https://doi.org/10.1016/j.epsl.2011.08.022

Herman, F., Beyssac, O., Brughelli, M., Brughelli, M., Leprince, S., Adatte, T., et al. (2015). Erosion by an Alpine glacier. *Science*, *350*(6257), 193–195. https://doi.org/10.1126/science.aab2386

Herman, F., & Brandon, M. (2015). Mid-latitude glacial erosion hotspot related to equatorial shifts in southern westerlies. *Geology*, *43*(11), 987–990. https://doi.org/10.1130/G37008.1

Hewitt, I. (2013). Seasonal changes in ice sheet motion due to melt water lubrication. *Earth and Planetary Science Letters*, *371*, 16–25.

Hildes, D. H., Clarke, G. K., Flowers, G. E., & Marshall, S. J. (2004). Subglacial erosion and englacial sediment transport modelled for North American ice sheets. *Quaternary Science Reviews*, *23*(3-4), 409–430. https://doi.org/10.1016/j.quascirev.2003.06.005

Hodge, S. M. (1974). Variations in the sliding of a temperate glacier. *Journal of Glaciology*, *13*(69), 349–369. https://doi.org/10.1017/S0022143000023157

Hooke, R. L. B. (2005). *Principles of glacier mechanics* (2nd ed., p. 448). New York: Cambridge University Press. https://doi.org/10.1017/CBO9780511614231

Hooke, R. L. B., Lauman, T., & Kohler, J. (1990). Subglacial water pressures and the shape of subglacial conduits. *Journal of Glaciology*, *36*(122), 67–71. https://doi.org/10.1017/S0022143000005566

Hooyer, T. S., Cohen, D., & Iverson, N. R. (2012). Control of glacial quarrying by bedrock joints. *Geomorphology*, *153*, 91–101.

Iken, A. (1981). The effect of the subglacial water pressure on the sliding velocity of a glacier in an idealized numerical model. *Journal of Glaciology*, *27*(97), 407–421. https://doi.org/10.1017/S0022143000011448

Iken, A., & Bindschadler, R. A. (1986). Combined measurements of subglacial water pressure and surface velocity of Findelengletscher, Switzerland: Conclusions about drainage system and sliding mechanism. *Journal of Glaciology*, *32*(110), 101–119. https://doi.org/10.1017/S0022143000006936

Iken, A., & Truffer, M. (1997). The relationship between subglacial water pressure and velocity of Findelengletscher, Switzerland, during its advance and retreat. *Journal of Glaciology*, *43*(144), 328–338. https://doi.org/10.1017/S0022143000003282

Iverson, N. (2012). A theory of glacial quarrying for landscape evolution models. *Geology*, *40*(8), 679–682. https://doi.org/10.1130/G33079.1

Iverson, N. R. (1990). Laboratory simulations of glacial abrasion: Comparison with theory. *Journal of Glaciology*, *36*(124), 304–314. https://doi.org/10.3189/002214390793701264

Iverson, N. R. (1991). Potential effects of subglacial water-pressure fluctuations on quarrying. *Journal of Glaciology*, *37*(125), 27–36. https://doi.org/10.1017/S0022143000042763

Iverson, N. R., Cohen, D., Hooyer, T. S., Fisher, U. H., Jackson, M., Moore, P. L., et al. (2003). Effects of basal debris on glacier flow. *Science*, *301*(5629), 81–84. https://doi.org/10.1126/science.1083086

Iverson, N. R., & Petersen, B. B. (2011). A new laboratory device for study of subglacial processes: First results on ice-bed separation during sliding. *Journal of Glaciology*, *57*(206), 1135–1146. https://doi.org/10.3189/002214311798843458

Jaeger, J., & Cook, N. (1979). *Fundamentals of rock mechanics* (p. 593). London: Chapman and Hall.

Jamieson, S. S. R., Hulton, N. R. J., & Hagdorn, M. (2008). Modelling landscape evolution under ice sheets. *Geomorphology*, *97*(1–2), 91–108. https://doi.org/10.1016/j.geomorph.2007.02.047

Kamb, B. (1987). Glacier surge mechanism based on linked cavity configuration of the basal water conduit system. *Journal of Geophysical Research*, *92*, 9083–9100. https://doi.org/10.1029/JB092iB09p09083

Kamb, B., Engelhardt, H., Fahnestock, M. A., Humphrey, N., Meier, M., & Stone, D. (1994). Mechanical and hydrologic basis for the rapid motion of a large tidewater glacier: 2. Interpretation. *Journal of Geophysical Research*, *99*, 15,231–15,244. https://doi.org/10.1029/94JB00467

Kessler, M. A., & Anderson, R. S. (2004). Testing a numerical glacial hydrological model using spring speed-up events and outburst floods. *Geophysical Research Letters*, *31*, L18503. https://doi.org/10.1029/2004GL020622

Kessler, M. A., Anderson, R. S., & Briner, J. P. (2008). Fjord insertion into continental margins driven by topographic steering of ice. *Nature Geoscience*, *1*(6), 365–369. https://doi.org/10.1038/ngeo201

Koppes, M., Hallet, B., Rignot, E., Mouginot, J., Wellner, J. S., & Boldt, K. (2015). Observed latitudinal variations in erosion as a function of glacier dynamics. *Nature*, *526*(7571), 100–103. https://doi.org/10.1038/nature15385

Krabbendam, M., & Bradwell, T. (2014). Quaternary evolution of glaciated gneiss terrains: Pre-glacial weathering vs. glacial erosion. *Quaternary Science Reviews*, *95*, 20–42. https://doi.org/10.1016/j.quascirev.2014.03.013

Lappegard, G., & Kohler, J. (2005). Determination of basal hydraulic systems based on subglacial high-pressure pump experiments. *Annals of Glaciology*, *40*(1), 37–42. https://doi.org/10.3189/172756405781813681

MacGregor, K. R., Anderson, R., Anderson, S., & Waddington, E. (2000). Numerical simulations of glacial-valley longitudinal profile evolution. *Geology*, *28*(11), 1031–1034. https://doi.org/10.1130/0091-7613(2000)28<1031:NSOGLP>2.0.CO;2

MacGregor, K. R., Anderson, R. S., & Waddington, E. D. (2009). Numerical modeling of glacial erosion and headwall processes in alpine valleys. *Geomorphology*, *103*(2), 189–204. https://doi.org/10.1016/j.geomorph.2008.04.022

Macgregor, K. R., Riihimaki, C. A., & Anderson, R. S. (2005). Spatial and temporal evolution of rapid basal sliding on Bench Glacier, Alaska, USA. *Journal of Glaciology*, *51*(172), 49–63. https://doi.org/10.3189/172756505781829485

Mair, D., Nienow, P., Willis, I., & Sharp, M. (2001). Spatial patterns of glacier motion during a high-velocity event: Haut Glacier d'Arolla, Switzerland. *Journal of Glaciology*, *47*(156), 9–20. https://doi.org/10.3189/172756501781832412

Müller, F., & Iken, A. (1973). Velocity fluctuations and water regime of arctic valley glaciers. *International Association of Scientific Hydrology. Publication*, *95*, 165–182.

Röthlisberger, H., & Lang, H. (1987). Glacial hydrology. In A. M. Gurnell & M. J. Clark (Eds.), *Glacio-fluvial sediment transfer. An alpine perspective* (pp. 207–284). New York: Wiley.

Schoof, C. (2005). The effect of cavitation on glacier sliding. *Proceedings of the Royal Society A: Mathematical, Physical and Engineering Science*, *461*(2055), 609–627. https://doi.org/10.1098/rspa.2004.1350

Schoof, C. (2010). Ice-sheet acceleration driven by melt supply variability. *Nature*, *468*(7325), 803–806. https://doi.org/10.1038/nature09618

Tomkin, J. H. (2009). Numerically simulating alpine landscapes: The geomorphologic consequences of incorporating glacial erosion in surface process models. *Geomorphology*, *103*(2), 180–188. https://doi.org/10.1016/j.geomorph.2008.04.021

Ugelvig, S. V., & Egholm, D. L. (2018). The influence of basal-ice debris on patterns and rates of glacial erosion. *Earth and Planetary Science Letters*, *490*, 110–121. https://doi.org/10.1016/j.epsl.2018.03.022

Ugelvig, S. V., Egholm, D. L., & Iverson, N. R. (2016). Glacial landscape evolution by subglacial quarrying: A multiscale computational approach. *Journal of Geophysical Research: Earth Surface*, *121*, 2042–2068. https://doi.org/10.1002/2016JF003960

Velde, B., Dubois, J., Moore, D., & Touchard, G. (1991). Fractal patterns of fractures in granites. *Earth and Planetary Science Letters*, *104*(1), 25–35. https://doi.org/10.1016/0012-821X(91)90234-9

Walder, J. S. (1986). Hydraulics of subglacial cavities. *Journal of Glaciology*, *32*(112), 439–445. https://doi.org/10.1017/S0022143000012156

Werder, M. A., Hewitt, I. J., Schoof, C. G., & Flowers, G. E. (2013). Modeling channelized and distributed subglacial drainage in two dimensions. *Journal of Geophysical Research: Earth Surface*, *118*, 2140–2158. https://doi.org/10.1002/jgrf.20146

Zahouani, H., Vargiolu, R., & Loubet, J.-L. (1998). Fractal models of surface topography and contact mechanics. *Mathematical and Computer Modelling*, *28*(4-8), 517–534. https://doi.org/10.1016/S0895-7177(98)00139-3